

Assessing albedo dynamics and its environmental controls of grasslands over the Tibetan Plateau

Lei Zheng^{a,b}, Youcun Qi^{a,b,*}, Zhangcai Qin^{c,d,**}, Xiaofeng Xu^e, Jinwei Dong^{b,f}

^a Key Laboratory of Water Cycle and Related Land Surface Processes, Institute of Geographic Sciences and Natural Resources Research, Chinese Academy of Sciences, Beijing 100101, China

^b University of Chinese Academy of Sciences, Beijing 100049, China

^c School of Atmospheric Sciences, Sun Yat-sen University, Key Laboratory of Tropical Atmosphere-Ocean System, Ministry of Education, Zhuhai 519000, China

^d Southern Marine Science and Engineering Guangdong Laboratory (Zhuhai), Zhuhai 519000, China

^e China Meteorological Administration, Beijing 100081, China

^f Key Laboratory of Land Surface Pattern and Simulation, Institute of Geographic Sciences and Natural Resources Research, Chinese Academy of Sciences, Beijing 100101, China

ARTICLE INFO

Keywords:

Albedo
Aridity
NDVI
Snow cover
Soil moisture
Grassland
Climate change

ABSTRACT

Land surface albedo, as an essential biophysical factor, plays an essential role in surface energy balance. Identifying environmental drivers of albedo in the Tibetan Plateau (TP) helps to understand the role of the “third pole” in responding to environmental change and regulating regional climate. Based on remotely sensed data of albedo, Normalized Difference Vegetation Index (NDVI), snow cover, and soil moisture, this study investigated the effects of land cover (i.e., vegetation, snow) and soil on albedo from the perspectives of spatial, temporal, and spectral (visible, near-infrared, and shortwave) changes of albedo. Generally, changes in shortwave (SW) albedo were primarily driven by changes in snow cover during the growing season (from May to September), predominantly in May and June. The NDVI had larger contributions to visible (VIS) albedo change and was identified as the foremost important driver for VIS albedo in July and August. The correlations between the near-infrared (NIR) albedo and NDVI were positive in the mid- and late growing season in eastern TP. Soil moisture was negatively correlated with albedo throughout the growing season and was identified as the foremost important driver in August. The NIR albedo was more susceptible than the VIS albedo to changes in soil moisture. The correlations between NDVI and albedo varied across different categories of aridity caused by changing correlations between NIR albedo and NDVI along the aridity gradients, and consequently the VIS and NIR albedo counterbalance can further limit the contributions of vegetation greenness on SW albedo in sub-humid and humid region. Our findings are expected to improve understandings of energy budget simulations over TP region in land surface models.

1. Introduction

Land surface albedo, defined as the ratio of the total radiation reflected from a surface to the total incident radiation that falls on it, is a critical variable in determining the land surface radiation budget (Bonan, 2008). Albedo is an essential biophysical factor for understanding of biophysical process. It directly impacts the surface energy balance and net radiation partitioning (Abera et al., 2019; Bright et al.,

2017; Chen et al., 2018; Wang et al., 2018a). Albedo is affected by numerous interrelated factors including snow cover (Fassnacht et al., 2016; Skiles and Painter, 2016), vegetation (Loranty et al., 2011; Lukeš et al., 2016; Planque et al., 2017; Tian et al., 2014), climate (Abera et al., 2020), and soil moisture (Li et al., 2018d; Sanchez-Mejia et al., 2014). Snow cover change provides a greater contribution to land surface albedo variation than do other factors due to its high reflectance (Moody et al., 2007). The albedo correlated with vegetation changes in rapid

* Corresponding author Youcun Qi at: Institute of Geographic Sciences and Natural Resources Research, Chinese Academy of Sciences, Key Laboratory of Water Cycle and Related Land Surface Processes, Datun Road No.11A, Chaoyang District, Beijing 100101, China.

** Corresponding author Zhangcai Qin at: School of Atmospheric Sciences, Sun Yat-sen University, Key Laboratory of Tropical Atmosphere-Ocean System, Ministry of Education, Zhuhai 519000, China.

E-mail addresses: youcun.qi@igsrr.ac.cn (Y. Qi), qinzhangcai@mail.sysu.edu.cn (Z. Qin).

<https://doi.org/10.1016/j.agrformet.2021.108479>

Received 6 June 2020; Received in revised form 27 March 2021; Accepted 11 May 2021

Available online 28 May 2021

0168-1923/© 2021 Elsevier B.V. All rights reserved.

spring transition (i.e., beginning of the growing season) has an important impact on surface energy budgets (Song, 1999). Precipitation and air temperature can influence the albedo through different mechanisms and subsequently change the amount of available energy at the land surface (Alibakhshi et al., 2019). For instance, increasing precipitation enhanced vegetation greenness and increased soil moisture, particularly in arid regions, causing changes in the albedo (Meng et al., 2017; Piao et al., 2012). Snow albedo is affected by the total amount of snowfall and the number of days with snowfall events, as fresh snow with small grains has a high albedo value and aged snow has a lower albedo (Seidel et al., 2016). Temperature impacts snow particle size, shape, and melting of snow, causing changes in albedo (Fassnacht et al., 2016; Malmros et al., 2018). Overall, vegetation, snow cover, and soil moisture directly affect albedo through land cover change and soil, while air temperature and precipitation affect albedo indirectly *via* vegetation growth, melting of snow, and soil moisture (Kala et al., 2014). The beginning of the growing season (BGS) indicates the start of the vegetation greening, which can indirectly affects albedo (Loranty et al., 2011).

Tibetan Plateau (TP), with massive areas covered with grasslands, plays a fundamental role in regulating carbon dynamics, biodiversity, and climate in China and surrounding regions (Li et al., 2018b; Tan et al., 2010; Xia et al., 2018). During the past several decades, TP has experienced dramatic climate change (e.g., warming and wetting) (Duan and Xiao, 2015; Wang et al., 2018b). Many studies have quantified the impact of climate change on grassland dynamics using statistical analysis, manipulative experiments and modeling methods (Chen et al., 2014; Ganjurjav et al., 2016; Li et al., 2019; Zhang et al., 2012), showing that climate warming induced greening in alpine meadows and browning in alpine steppes, while the increasing precipitation (wetting) caused increased biomass over TP grasslands. The monthly snow cover experienced a large spatiotemporal heterogeneous change in growing season and showed decreasing trends for most of TP in May, which indicated an early melting of snow (Li et al., 2018a). The soil moisture in TP with significant increasing trends was concentrated mainly in the central parts caused by the increasing precipitation (Bai et al., 2019). The factors mentioned above affect albedo through combined effects and consequently change the energy budget. In addition, the highest value of snow albedo radiative forcing occurs in TP, since TP is located at relatively low latitude with much more insolation than the higher latitudes and until relatively late spring snow may persist (Xiao et al., 2017).

Previous studies found a significant negative correlation between vegetation changes and land surface albedo during the growing season in the grassland of TP using Normalized Difference Vegetation Index (NDVI) (Shen et al., 2015; Tian et al., 2014). The correlations between albedo and vegetation greenness also represent temporal variability within the growing season (Zheng et al., 2019). These studies have well detected explicit correlations between albedo and vegetation, but it is unclear how snow cover, vegetation, and soil moisture affect the albedo at monthly scale by competing effects. Especially that regional trend of albedo change may still vary depending on the spatial and temporal resolution of specific analysis (Tian et al., 2014). In addition, many studies focused on total albedo with few attentions to its subsets.

Land surface albedo is the amount of the diffuse reflection of solar radiation, which is shortwave (SW) electromagnetic radiation generally within 0.3–5.0 μm range. Within this SW spectrum, the visible (VIS, 0.3–0.7 μm) and near-infrared (NIR, 0.7–5.0 μm) broadbands are frequently considered separately due to the green vegetation reflectance of NIR is much higher than that of VIS (Kuusinen et al., 2016). Additionally, the opposite changes in VIS and NIR albedo may cancel each other, restricting changes in total SW albedo (Abera et al., 2020). Aside from the vegetation, soil background influences albedo directly or indirectly (Abera et al., 2020; Carrer et al., 2014). The TP region experiencing arid, semi-arid, semi-humid, and humid gradients from the northwestern to the southeastern areas (Gao et al., 2015) needs to be examined for its soil background impacts on albedo.

Therefore, in this study, we examined both spatial and temporal changes of albedo, and further analyzed a full set of potential drivers including climate, BGS, snow cover, vegetation greenness and soil moisture. The intention of the study was to understand the interactions among albedo, climate and land surface changes that could help biophysical simulations in TP region.

Specifically, using growing season monthly data during 2000–2018 (2017 for soil moisture and 2015 for BGS) in TP region, we first detected spatial and temporal trends in albedo, snow cover, vegetation greenness, and soil moisture, then identified correlations between albedo and snow cover, vegetation greenness, soil moisture, precipitation, air temperature, and BGS. Finally, we examined dependencies of correlations between albedo and environmental factors with respect to aridity.

2. Data and methods

2.1. Study area

The Tibetan Plateau (TP), also known as the Qinghai-Tibetan Plateau, is “the third pole” of Earth with an average altitude of over 4000 m. The climate of the Tibetan Plateau (TP) is controlled by the Indian summer monsoon in the summer and westerlies in the winter (Yao et al., 2012). The mean annual temperature ranges from -15°C to 5°C (You et al., 2013). Precipitation in the region mainly occurs in the summer with annual precipitation in the grassland of TP showing a southeastward increasing pattern ranging from 100 to 700 mm (Yang et al., 2010b). The annual mean snow cover fraction over the TP is 17.16% and high snow cover fraction values are mainly distributed in the upper reaches of the Tarim River, Brahmaputra River, and Mekong River basins (Chen et al., 2017). The annual mean snow-covered duration over the TP is 57 days and snow-covered melt is at the end of March from 2000 to 2015 (Wang et al., 2017b). The grassland type varies along the precipitation gradient from alpine meadow in the east, to alpine steppe in the central area, and desert grassland in the west (Wu et al., 2013). In TP region, the growing season is normally from May to September (Shen et al., 2015; Tian et al., 2014).

2.2. Data

2.2.1. Grassland cover data

The extent of the grassland was defined by using annual land cover type products (MCD12C1.006) of the Moderate Resolution Imaging Spectroradiometer (MODIS) at a 0.05° spatial resolution with the International Geosphere-Biosphere Program (IGBP) land cover scheme (Friedl et al., 2010). We defined grassland pixels as those pixels which were classified as grassland > 90% of the time between 2001 and 2017 to avoid the disturbance from land cover changes.

2.2.2. Vegetation greenness data

Vegetation greenness with a spatial resolution of 0.05° was obtained from the MODIS/Terra monthly NDVI product (MOD13C2, Collection 6), which was based on cloud-free spatial composites of 16 day, 1 km NDVI data. Data was used for the period 2000 to 2018. In this study, only the grid cells with NDVI greater than 0.1 were used in order to eliminate the influence of bare and sparsely vegetated regions during the growing season (Li et al., 2018c). All cloud contaminated, snow covered and estimated pixels were filtered and removed from our analysis using pixel reliability flag values (i.e., using pixel reliability flag only pixels identified bits = 0 and 1 were used).

2.2.3. Albedo data

The albedo data was obtained from the MODIS daily albedo product (MCD43C3, Collection 6). The daily albedo product used here has a spatial resolution of 0.05° and was temporally aggregated to a monthly scale by taking the average of all daily retrievals in each month to match the other data. We filtered and removed values with band quality 5 (50%

or more fill values). We used VIS (0.3–0.7 μm), NIR (0.7–5.0 μm), and total SW (0.3–5.0 μm) broadband white-sky albedo. The improvements in the MODIS Collection 6 MCD43C3 using improved MODIS reflectance, cloud masking, and daily inversion algorithm (Wang et al., 2018c) may allow the use of MCD43C3 data to detect dynamics of short-term variable snow cover that contribute to albedo changes.

2.2.4. Snow cover data

The snow cover dataset (MOD10CM.006) from 2000 to 2018 was obtained from National Snow and Ice Data Center with a spatial resolution of 0.05° and a monthly temporal resolution, and with the unit of percent per pixel. Depending on the study area, season and validation process, the accuracy of MODIS snow cover products was between 85% and 95%, and the accuracy of snow cover is generally higher for grassland than that of forest (Coll and Li, 2018).

2.2.5. Soil moisture data

The Climate Change Initiative (CCI) dataset of the European Space Agency (ESA) is adopted for monitoring the global trend in soil moisture and was obtained from the ESA website. The ESA CCI soil moisture product, which combined multiple single-sensor active and passive microwave soil moisture products by ESA, is a global daily soil moisture product with a spatial resolution of 0.25° (Dorigo et al., 2017). The ESA CCI v4.4 dataset combined (active-passive) soil moisture product directly generated from various active and passive product was used in this study, covering the period 2000–2017. The daily soil moisture product was temporally aggregated to a monthly scale to match the other data by taking the average of all daily values in each month.

2.2.6. Precipitation, temperature, phenology, and aridity index data

Global Satellite Mapping of Precipitation for Global Precipitation Measurement (GSMaP)-Gauge v7 has been developed by JST and JAXA. It combines several Passive Microwave (PMW) and IR sensor data to produce 0.1° resolution satellite-based precipitation product. This is a daily precipitation product with a time span from 2000 to 2018. The daily value was temporally aggregated to a monthly scale to match the other data by taking the average of all daily values in each month. The monthly mean temperature dataset CRU 4.02 a climate dataset with a spatial resolution of 0.5° spanning 2000 to 2018, was obtained from the Climate Research Unit (CRU) at the University of East Anglia. Variations in the vegetation BGS due to climate change will have potential impacts on albedo and most of the TP experienced a continuous advancing trend in the BGS, therefore we add BGS to our analysis (Wang et al., 2017a). The phenology data was obtained from the Vegetation Index and Phenology (VIP) Vegetation Indices Monthly Global datasets (version 4), which was developed by the VIP Research Lab at the University of Arizona, with a spatial resolution of 0.05° (Didan and Barreto, 2016). This is a yearly phenology product with a time span from 1982 to 2015. This product includes the start of season, the end of season, and the day of peak. We used the data of start of season during 2000–2015. Given the large spatial variations of precipitation over the TP, the aridity index was used to divide the study region into four aridity categories. The aridity index was obtained from the Global Aridity Index and Potential Evapotranspiration (ETO) Climate Database v2.

2.3. Methods

2.3.1. Linear regression analysis

The trends of NDVI, snow cover, soil moisture, and albedo were calculated using the linear regression at the pixel scale. The analyses of the pixel scale revealed the spatial patterns of the albedo and environmental factors. For temporal scales, analyses were conducted in the growing season at a monthly step (i.e., each month in the growing season). The trend was calculated as the slope of linear regression using the ordinary least squares method:

$$\text{Slope} = \frac{n \times \sum_{i=1}^n (i \times A_i) - \sum_{i=1}^n i \times \sum_{i=1}^n A_i}{n \times \sum_{i=1}^n i^2 - \left(\sum_{i=1}^n i \right)^2} \quad (1)$$

where n was the length of the time series that was studied ($n = 19$, 18 for soil moisture); i was the number of year; and A_i was albedo and environmental factors in the i th year. From the time series images of albedo and environmental factors, we calculated the regression slope and the p -value for each pixel. Thus, we created maps of increasing or decreasing trends in NDVI, snow cover, soil moisture, and albedo by using the positive or negative slopes.

2.3.2. Correlation analysis and partial correlation analysis

Aggregation groups rectangular areas to create larger pixels. The albedo (0.05°) was aggregated to a lower resolution (0.1° and 0.5°) with mean function to match that of precipitation and temperature. Due to the temporal differences in data sources, not all pixels have complete time series data for analysis in each month of the growing season (Fig. S1). To ensure data quality, correlation analysis was only carried out for pixels with valid values of more than 10 years. To investigate the impacts of precipitation, temperature and begin of the growing season on albedo, we calculated the Pearson's correlation coefficient (r) for precipitation, temperature, and BGS with albedo (SW, NIR, and VIS) for each month (only May for BGS) of the growing season from 2000 to 2018 (2015 for BGS):

$$r_{xy} = \frac{\sum_{i=1}^n (x_i - \bar{x})(y_i - \bar{y})}{\sqrt{\sum_{i=1}^n (x_i - \bar{x})^2 \sum_{i=1}^n (y_i - \bar{y})^2}} \quad (2)$$

where x_i and y_i were the values of the i th year, \bar{x} and \bar{y} were the average values of the all years. When $r > 0$, the two variables were positively correlated, and when $r < 0$, the two variables were negatively correlated. For each month of growing season, the correlation analyses were performed between one factor (i.e., precipitation or temperature) with albedo. Thus, we obtained the variation of correlation between one factor (i.e., precipitation or temperature) with albedo within the growing season.

To understand the potential role of environmental drivers (i.e., snow cover, soil moisture, greenness) in albedo change, we perform partial correlation analysis instead of the Pearson's correlation to isolate potential correlations among drivers. We aggregate the raster of albedo, NDVI, and snow cover fraction (SCF) to a lower resolution to match soil moisture (0.25°). The values for resulting cells is computed with mean function. Partial correlation analysis was also only carried out for pixels with valid values of more than 10 years. All variables are detrended to isolate the role of NDVI, snow cover, soil moisture from other drivers/mechanisms that contribute to albedo dynamics. The formula is as follows:

$$r_{12,3\sim p}^2 = \frac{R_{1(2,3,\dots,p)}^2 - R_{1(3,\dots,p)}^2}{1 - R_{1(3,\dots,p)}^2} \quad (3)$$

Where $r_{12,3\sim p}$ refers to the partial correlation coefficient of variables 1 and 2; $R_{1(2,3,\dots,p)}^2$ is the determination coefficient of the regression analysis of variable 1 and variable (2~ p); and $R_{1(3,\dots,p)}^2$ refers to the determination coefficient of the regression analysis of variable 1 and variable (3~ p). For example, to calculate the partial correlation coefficient of albedo to NDVI, $r_{12,3\sim p}$ refers to the partial correlation coefficient of albedo and NDVI, which uses snow cover and soil moisture as control variables. $R_{1(2,3,\dots,p)}^2$ is the determination coefficient of the regression of albedo, NDVI, snow cover, soil moisture; and $R_{1(3,\dots,p)}^2$ refers to the determination coefficient of the regression of albedo and snow cover and soil moisture.

2.3.3. Relative importance of NDVI, snow cover and soil moisture to albedo change

We used a relative importance analysis approach to quantify the relative contributions of vegetation greenness, snow cover and soil moisture to albedo changes in each grid cell, expressed as the Pearson correlation in a multiple linear regression ($albedo = b_0 + b_1 \times NDVI + b_2 \times snow\ cover + b_3 \times soil\ moisture + \varepsilon$). ε represented other factors that might contribute to albedo variation. Relative importance analysis was only carried out for pixels with valid values of over 12 years. The analysis was conducted using the ‘relaimpo’ package in R, which was based on decomposition of variance for multiple linear regression models. One of the most computer-intensive and commonly used methods named ‘LMG’ was chosen to differentiate contributions of different correlated regressors in a multiple linear regression (Grömping, 2006). The contribution of NDVI, snow cover, and soil moisture in each grid cell across the study area were quantified, and then the higher contribution to the albedo variation was identified as the dominant driver (Hou et al., 2018; Huang et al., 2018).

3. Results

3.1. Spatial and temporal patterns

Fig. 1 illustrated the spatial distribution of annual growing season means of albedo, NDVI, SCF, and soil moisture over 2000–2018 (2017 for soil moisture hereafter). The mean SW albedo, NDVI, SCF, and soil moisture in grasslands of TP were 0.18, 0.39, 3.6%, and $0.25\text{ m}^3/\text{m}^3$, respectively. There was a strong pattern of decreasing NDVI from southeastern to northwestern portion of grasslands of the TP (Fig. 1b), which was spatially coherent with that of soil moisture (Fig. 1d). In accordance with the vegetation greenness and soil moisture gradient, the SW albedo increased from approximately 0.1 to 0.4 along the gradient from southeast to northwest (Fig. 1a). The spatial fields of annual growing season means of NIR and VIS albedo were shown in Fig. S2. Snow cover mainly distributed in mountain areas with relatively

high altitude with the highest value of SCF reaching 38.7% (Fig. 1c). Fig. 2 presented the intra-annual cycles of SW albedo, NDVI, SCF, and soil moisture averaged over the grasslands of the TP, showing strong seasonal variations in the growing season. The means of SW albedo were 0.22 (May), 0.18 (June), and 0.17 (July–September), respectively (Fig. 2a). The NIR and VIS albedo exhibited distinct intra-growing season variability. NIR albedo fluctuated slightly in different months of the growing season, and it was approximately 0.25 in each month of the growing season. In contrast, the VIS albedo showed the maximum value in May (0.17), with the minimum value in July and August (0.08). The grasslands presented larger NDVI in July and August, with the maximum NDVI in August (0.47). The lowest NDVI appeared in May (0.24), about half of that in July and August (Fig. 2b). On the contrary, the grasslands showed the highest SCF in May (12.0%), which was more variable than other months (Fig. 2c), and presented much lower SCF at the peak of the growing season (1.2–1.4% in July–August). Similar to NDVI, the lowest soil moisture appeared in May ($0.22\text{ m}^3/\text{m}^3$), then increased until July with an average of $0.26\text{ m}^3/\text{m}^3$ during July to September (Fig. 2d).

The SW albedo, NDVI, SCF, and soil moisture varied spatially across the grasslands of TP during 2000–2018 (Fig. 3). An increased SW albedo was observed for 27.3% of the pixels, mainly in the northwest and east of the TP (Fig. 3a). Of these positive trends, 85.0% were between 0 and 0.0005 year^{-1} . Significant ($p < 0.05$ hereafter) positive trends in SW albedo were found in only 2.4% of the pixels. Negative trends in SW albedo were found in 72.7% of the pixels, mostly in the center-south of the TP, with 76.7% ranging between 0 and -0.001 year^{-1} . About 20.1% of the total investigated pixels showed significant decreases in SW albedo. When comparing the trends of NIR and VIS albedo, 35.8% and 13.2% of grasslands experienced increasing trends, respectively (Fig. S3). The accelerated decreasing trend of albedo was found in May relative to the other months (Fig. S4). For instance, the decreased SW albedo was observed in 73.5% of the pixels, with 53.0% below -0.001 year^{-1} (Fig. S4a1). The NDVI trend patterns were spatially heterogeneous from 2000 to 2018 (Fig. 3b), but the mean NDVI of the TP increased. The NDVI exhibited greening trends in 74.9% of the total

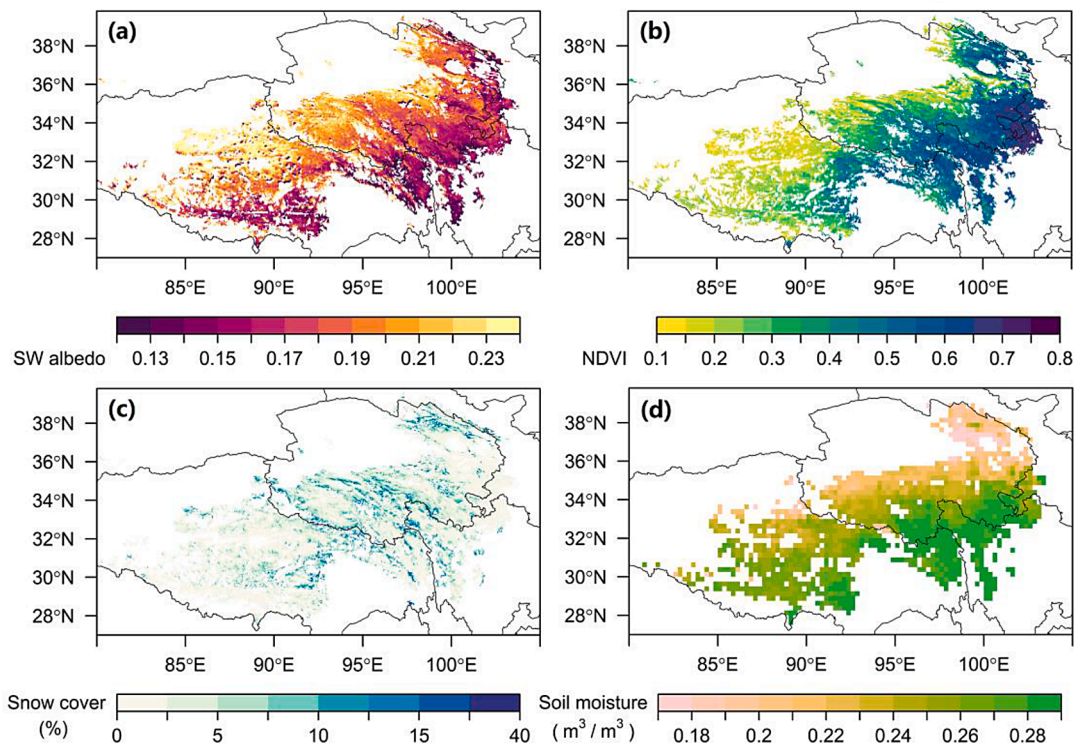


Fig. 1. Spatial distribution of growing season averages of the shortwave (SW) albedo (a), NDVI (b), snow cover fraction (c), and the soil moisture (d) over the grasslands in Tibetan Plateau (TP) during 2000–2018 (2017 for soil moisture).

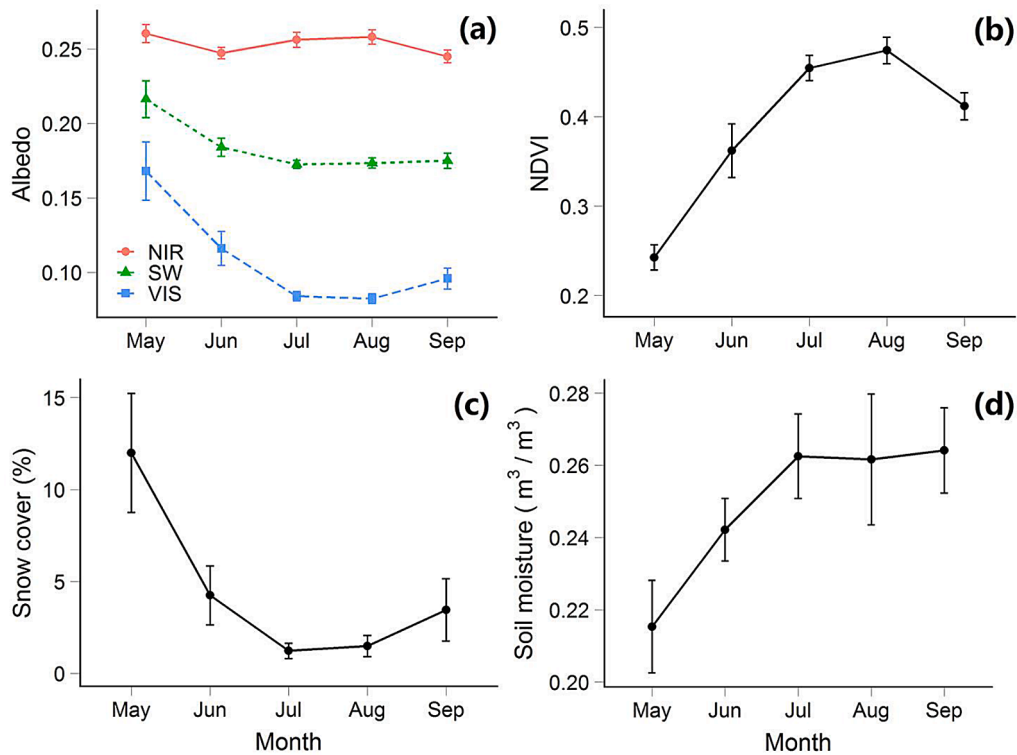


Fig. 2. Intra-growing season variability of SW albedo (a), NDVI (b), SCF (c), and the soil moisture (d) over the grasslands in TP during 2000–2018 (2017 for soil moisture). The error bars expressed as the standard deviation in a given month.

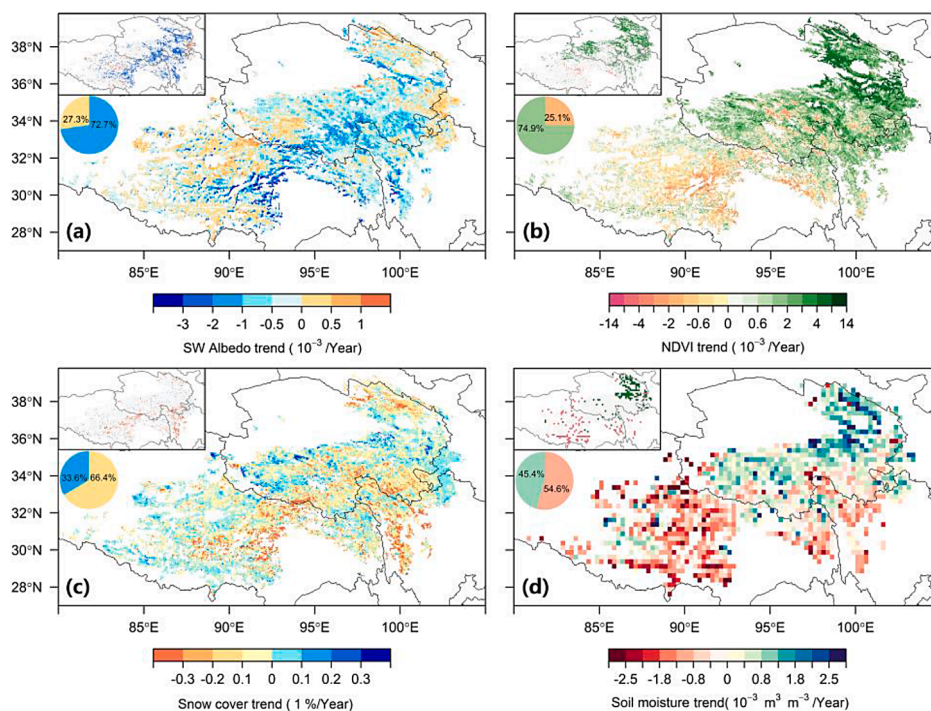


Fig. 3. Spatial pattern of trends in growing season mean SW albedo (a), NDVI (b), snow cover fraction (c), and soil moisture (d) over the grasslands in TP during the period 2000–2018 (2017 for soil moisture). The inset panels show the pixels with statistical significance ($p < 0.05$). The inset pie charts show the area fractions of lands with uptrend and downtrend respectively.

investigated pixels (25.2% significantly), primarily located in eastern and northern areas of the TP. About 12.4% of grasslands characterized by the greening trend over 0.003 year^{-1} , which was mainly located in the northeast part of TP. On the contrary, 25.1% of the grasslands

displayed browning trends, primarily in the southwest TP, but most of these trends were not significant; only 2.3% of grasslands characterized by a browning trend below -0.003 year^{-1} , which sparsely distributed within local areas of the southwest TP. Notably, the NDVI trends varied

in different months of the growing season (Fig. S5). Specifically, the majority of the grasslands (79.3% and 80.1%) experienced an increasing trend in May and June, while only 67.1% and 62.5% of the grasslands experienced an increasing trend in August and September (Fig. S5a1-a5). The SCF trend showed large spatial heterogeneity over the study area (Fig. 3c). For SCF, 66.4% of grasslands experienced decreases, and mainly distributed in the center-southeast of the TP; and 5.6% of pixels were statistically significant for SCF decreasing. Meanwhile, 33.6% of grasslands showed increasing trends in SCF. Of these grasslands, 0.8% had statistically significant increasing trends. In May, 70.7% of the grasslands showed decreasing trends in SCF, with most (60.7%) of the negative trends below $-0.2\% \text{ year}^{-1}$ (Fig. S5b1). The decreasing albedo in May was in accord with the change in SCF (Fig. S5b1, Fig. S4a1). For soil moisture, both increased and decreased soil moisture were widespread (45.4% and 54.6%, respectively), and 10.6% and 8.6% of pixels were statistically significant for increasing and decreasing, whereas the increased soil moisture mainly appeared in the northeastern part of the TP, which was spatially coherent with vegetation greening of the TP (Fig. 3d). The decreased soil moisture dominated the west of the TP with less significance. There were strong intra-growing season variations in soil moisture for the study domains; the decreasing trends dominated the study area (71.3%) in August (Fig. S5c4).

3.2. SW albedo responding to climate

We observed widespread positive correlations between SW albedo and precipitation in May, with 70.3% (10.7%) of the investigated pixels (showing significantly), and negative correlation over 29.7% (1.7%) of the investigated pixels (showing significantly) (Fig. 4a). Correlations between the SW albedo and precipitation shifted from positive to negative from May to September (Fig. S6a1-a5). By August, the negative correlation became dominant, with 82.7% (36.6%) pixels showing (significant) negative correlations (Fig. S6a4). For temperature and SW albedo, both positive and negative correlations were widespread in May. However, there were both significant positive and negative correlations in less than 5.0% of the pixels (Fig. 4b). The correlation between temperature and SW albedo in other months was similar to that in May (Fig. S6b1-b5). We further examined the spatial pattern of correlation between BGS and SW albedo. For 61.7% of the pixels, BGS was positively correlated with SW albedo (meaning that the delayed growing season brings high albedo), but only less than 5.0% of the pixels were significant.

3.3. Land surface and soil controls on albedo

Here, we assessed to what extent albedo in grasslands of TP was driven by vegetation greenness, snow cover, and soil moisture. Based on a relative importance algorithm (see Methods) to attribute the change in albedo to its drivers (vegetation greenness, snow cover, and soil moisture), we constructed maps of the relative contributions of the major

control factors influencing albedo in each month of growing season (Fig. S8-S10). Snow cover was identified as the foremost important driver in May and June (Fig. 5d1-d2). For instance, in the May and June, 96.2% and 80.5% (80.5% and 43.6%) of the studied region demonstrated a positive (significant) correlation with snow cover. In contrast, only about 0.08% and 1.8% of the pixels exhibited significant negative correlation with snow cover in May and June, respectively. The main environmental control identified in NIR and VIS albedo (Fig. S11a1-a2, b1-b2) was broadly similar to that found in SW albedo, indicating the important role of snow cover in controlling albedo dynamics in May and June. In contrast to snow cover, NDVI used for denoting vegetation greenness was much less correlated with SW albedo particularly in May, June and September (Fig. 5a1, a2, a5). Viewed at regional level, NDVI was negatively correlated with SW albedo in northwestern areas of TP and positively correlated with SW albedo in southeastern areas of TP, especially in July and August (Fig. 5a3, a4). In July, August and September, the positive correlations between NIR albedo and NDVI became dominant, with 60.2%, 61.6% and 60.6% (17.3%, 17.8% and 13.9%) of pixels showing a (significant) positive correlation (Fig. S12a3-a5). The negative correlation between the VIS albedo and NDVI was stronger than that of NIR albedo. More specifically, about 93.8%, 93.4% and 83.7% (57.7%, 52.4% and 26.1%) of the pixels exhibited a (significant) negative correlation between VIS albedo and NDVI in July, August, and September, respectively (Fig. S13a3-a5). Considering the importance of NDVI in the VIS albedo, vegetation greenness was identified as a dominant control in July and August for VIS albedo (Fig. S11b3, b4). For soil moisture, in August and September, the negative correlation between soil moisture and SW albedo was widespread (91.5% and 93.9%), and 54.6% and 47.6% of investigated pixels were significant (Fig. 5c4, c5). Based on the spatial distribution of dominant environmental factors, soil moisture was identified as the foremost important driver in August (Fig. 5d4). Compared with VIS albedo, the impact of soil moisture on NIR albedo was stronger. The significant negative correlations characterized 29.7%, 61.6%, and 48.1% of the pixels between NIR albedo and soil moisture in July, August, and September (Fig. S12c3-c5), respectively, while the corresponding values of VIS albedo were 10.4%, 29.7%, and 35.1%, respectively (Fig. S13c3-c5). In July and September, for SW albedo, there was no single foremost important driver. In July, the area dominated by vegetation greenness was almost the same as soil moisture (Fig. 5d2), and in September, the area dominated by snow cover was almost the same as soil moisture (Fig. 5d5). This was mainly due to the VIS and NIR counterbalance, limiting the SW albedo to be controlled by any single factor (Fig. S11).

3.4. The role of aridity

To further explore the dependency of the albedo on the NDVI, snow cover, and soil moisture at any given location, we calculated the relative importance index (RI, higher RI suggesting greater importance, see Methods) and partial correlation coefficients for albedo with these

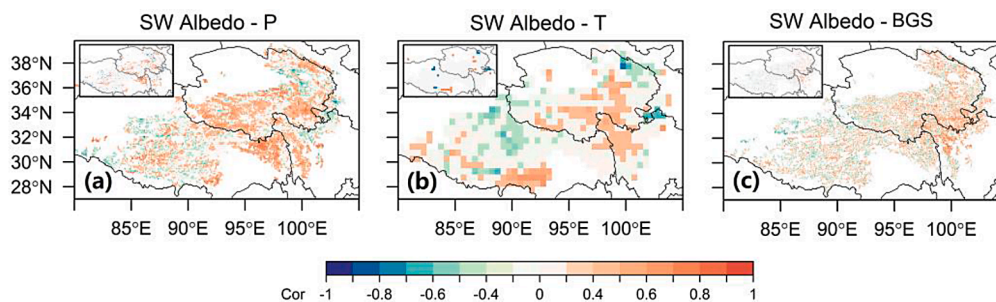


Fig. 4. Correlation coefficients between the SW albedo and the precipitation (a), temperature (b), and beginning of the growing season (c) over the grasslands in TP in May during the period 2000–2018 (2015 for BGS). The insets show the pixels with statistical significance ($p < 0.05$). P, T and BGS represent precipitation, temperature, and beginning of the growing season, respectively.

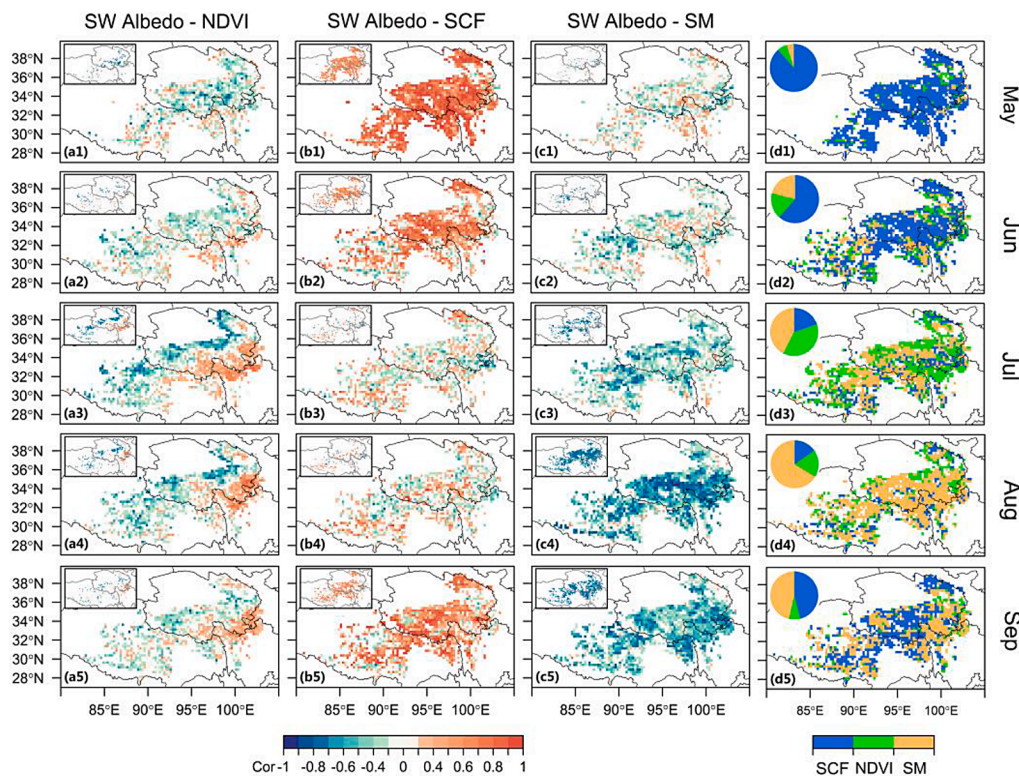


Fig. 5. Spatial distributions of the partial correlation coefficients between growing season monthly SW albedo and NDVI (a1-a5), snow cover fraction (b1-b5), and soil moisture (c1-c5), and spatial distribution of dominant constraints on SW albedo (d1-d5) over the grasslands in TP from May to September during the period 2000–2017. The inset panels show the pixels with statistical significance ($p < 0.05$). The inset pie charts show the area fractions of lands dominated by each factor. SCF and SM represent snow cover fraction and soil moisture, respectively.

environmental factors across the grasslands of TP. The results were grouped into four aridity categories according to aridity index (AI), namely arid ($AI < 0.2$), semi-arid ($0.2 < AI < 0.5$), dry sub-humid ($0.5 < AI < 0.65$), humid ($AI > 0.65$) (Fig. 6). In July and August, the contributions of NDVI to SW albedo were more important in arid and semi-arid regions than in dry sub-humid and humid regions. Positive correlations between NDVI and SW albedo mainly appeared in dry sub-humid and humid region, and the negative correlation dominated the arid and semi-arid region in July and August. The analysis demonstrated that the vegetation greening could decrease the albedo in the drier region and increase the albedo in the wetter region in July and August. In July and August, the NIR albedo significantly positively correlated with NDVI in dry sub-humid and humid region (Fig. S14), compared to SW albedo. Meanwhile, significant negative correlations between VIS albedo and NDVI were observed along the gradients of aridity in almost all

months (Fig. S15). A notable RI was observed in May for snow cover, which showed that snow cover played a more important role than NDVI and soil moisture in May. For soil moisture, its RI was enhanced along the gradients of aridity (from wetter to drier), which was more apparent in NIR albedo than in VIS albedo (Fig. S14, S15). Unlike the snow cover, the soil moisture exerted greater influence in the first half of the growing season than in the second half.

4. Discussion

4.1. Attribution of albedo changes to NDVI, snow cover, soil moisture from different perspectives of space, time and spectral bands

This study examined the complex correlations between land surface albedo with NDVI, snow cover, and soil moisture in grasslands of TP for

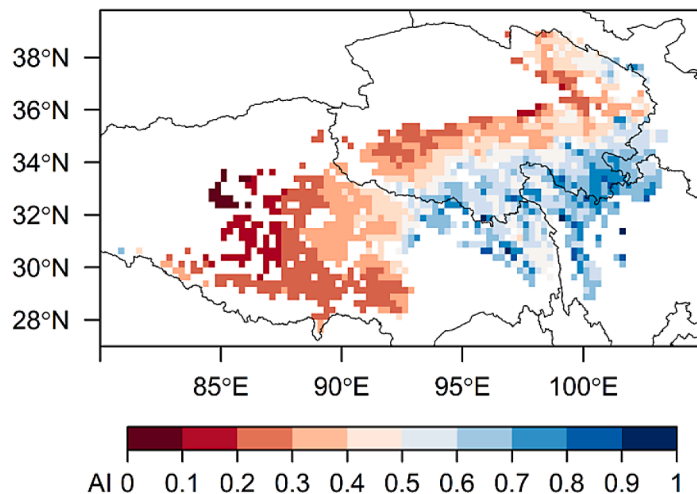


Fig. 6. Distribution of aridity index (AI) over grasslands in TP.

different broadbands of albedo (SW, VIS, and NIR) over each month of the growing season (from May to September). Generally, the change in SW albedo was in well agreement with the change in snow cover (Fig. 3a, c); the SW albedo strongly and positively correlated with snow cover in May, July, and September (Fig. 5b1, b2, b5). This can be partly related to the considerable snow cover existed in the May, July, and September (Li et al., 2018a; Pu et al., 2007). These results were based on monthly dynamics, different from growing season-based studies that reported vegetation greenness as the foremost import driver (Tian et al., 2017; Tian et al., 2014; Zheng et al., 2019).

In this study we found more details about monthly variation in the albedo-NDVI relationships during the growing season. Specifically, the correlations between the NIR albedo and NDVI changed from being negative in May to positive in other months in east of the grasslands (Fig. S12a1-a5). The VIS albedo was consistently negatively correlated with NDVI in most of the grasslands (Fig. S13a1-a5) and most of grasslands showed a significant negative correlation between VIS albedo and NDVI in July and August (Fig. S13a3, a4), which indicated that the VIS albedo was more susceptible to changes in vegetation greenness in the middle growing season. The NDVI contributed more to changes of VIS albedo (Fig. S10a3-a4) and was identified as the foremost important driver in July and August for VIS albedo (Fig. S11b3-b4), which provides supporting evidence for the important role of NDVI in VIS albedo in the middle growing season. The opposing relationship between VIS and NIR albedo with NDVI limited the pixels that had significant correlations between NDVI and SW albedo (Fig. 5a3-a5). This phenomenon is consistent with the previous findings in grasslands of TP (Zheng et al., 2019). The reason for NIR albedo being positively correlated with NDVI can be related to the increased multiple scattering within the canopy with relatively high leaf area index (LAI) (Abera et al., 2019; Gates, 1965; Hammerle et al., 2007). Contrary to the east of TP, the NIR albedo negatively correlated with NDVI in the north and northwest of TP (Fig. S12a2-a5). This indicates that the variations of NIR albedo in these grasslands were not driven by the change of scattering resulted from vegetation greening or browning, and can be explained by the change of fractional area covered by vegetation and background soil (Zheng et al., 2019). More specifically, increasing canopy cover rapidly covers bare soil and decreases the contribution of bare soil albedo to the overall surface albedo, resulting in negative correlation between NIR albedo and NDVI, and this phenomenon occurs in areas where LAI is low (shown by pattern of decreasing NDVI from southeastern to northwestern, Fig. 1b). The consistent negative relationship between VIS albedo and NDVI showed vegetation stress and reduced production of chlorophyll for photosynthesis, which could result in less absorption in the blue and red spectral regions (Abera et al., 2020).

Snow cover was identified as the foremost important driver in May and June (Fig. 5d1-d2). The changes of precipitation and temperature had impacts on snow cover and snow albedo (Malmros et al., 2018). Snow cover, which was directly related to the seasonal snowpack, is an important part of the energy budget due to its high albedo (Stewart, 2009). Reductions in the overall amount of precipitation as snow should likely decrease the depth of the snowpack and could potentially decrease the persistence of snow cover that could decrease the overall albedo (Fassnacht et al., 2016). Malmros et al. (2018) showed the negative correlation between snow albedo and air temperature in central Andes of Chile and Argentina. Our results showed that precipitation positively correlated with albedo in most of grasslands in TP in May (Fig. 4a). However, in June, the areas with positive correlations shrank (Fig. S6a2), and in July and August, precipitations negatively correlated with albedo in most of grasslands in TP (Fig. S6a3, a4). Our results revealed that precipitation impacts albedo through snow cover in the early growing season, and through soil moisture and vegetation in the late growing season. Our results indicated that changes in albedo may mainly be affected by changes in snow cover due to changes in precipitation, rather than temperature-induced snow melting in TP in the early growing season (Fig. 4b). The precipitation increased mainly in spring,

while regional mean precipitation showed an increase in other seasons, but with small and insignificant trends in 1961–2012 (Wang et al., 2018b). However, precipitation generally shows decreasing trends in May in 2000–2014, suggesting that the decrease in SCF was due to precipitation decrease in May (Li et al., 2018a). Therefore, the precipitation dynamics due to climate change will have incremental potential impacts on albedo and surface energy budgets, especially in early growing season.

In terms of soil moisture, albedo is negatively correlated to soil moisture content in all wavelengths (i.e., with a decrease in soil moisture, soil albedo increases and vice versa) (Abera et al., 2020; Li et al., 2018d; Zhang et al., 2013b). The soil moisture was negatively correlated with albedo throughout the growing season and was identified as the foremost important driver in August (Fig. 5c3-c5, d4). The NIR albedo, rather than the VIS albedo, was more susceptible to changes in soil moisture (Fig. S11). This result differs from previous study conducted in bare soils (Li et al., 2018d). Li et al. (2018d) showed larger correlation coefficients between VIS albedo and soil moisture than that between NIR albedo and soil moisture. The vegetation mainly absorbed radiance in VIS spectral regions, and reduced the impacts of soil moisture on VIS albedo. This indicates that SW albedo changes in grasslands of TP were driven by both vegetation and soil moisture variations in the middle growing season. Soil moisture contributed more to NIR albedo and vegetation contributed more to VIS albedo (Fig. S11a3-4, b3-4). Meng et al. (2017) showed that ESA soil moisture product significantly correlated with the observed precipitation in the TP. The significant correlation between precipitation and albedo in the middle and late growing season (Fig. S6a3-a5) provided supporting evidence that soil moisture plays an important role in regulating albedo in the grasslands of TP.

As for different aridity categories, the correlation between albedo and NDVI varied in grasslands of TP. In the dry sub-humid ($0.5 < AI < 0.65$) and humid ($AI > 0.65$) region, NDVI significantly ($p < 0.1$) positively correlated with SW albedo in August, while there were significant negative correlations between SW albedo and NDVI in arid region in July and August (Fig. 7). This difference across hydroclimatic variations can be explained by different correlations between NIR albedo and NDVI along the aridity gradients (Fig. S14, S15). In dry sub-humid and humid regions, expanding leaves and increasing canopy increased optical scattering/reflectance in the NIR spectral region (Abera et al., 2020; Williamson et al., 2016; Zheng et al., 2019). Contrary to the dry sub-humid and humid region, there were insignificant negative correlations between NIR albedo and NDVI in arid region (Fig. S14). This can be related to the change in the bare soil fraction caused by vegetation greening, i.e., the variation of LAI will directly change the contribution of soil albedo to the total surface albedo (Liu et al., 2017; Zheng et al., 2019). In arid region, less soil will be exposed with vegetation greening, thus the NIR albedo may decrease depending on the variation of bare soil fraction rather than optical scattering effects (Abera et al., 2020; Liu et al., 2017). The counterbalance between VIS and NIR albedo can further limit the contributions of vegetation greenness on SW albedo in sub-humid and humid region (Fig. 7). For snow cover, there were no differences along the aridity gradients. The snow cover contributed more in SW albedo in May than in other months (Fig. 7). Snow cover contributed more to VIS albedo than NIR albedo (Fig. S14, 15), similar to the temporal evolution in spectral snow albedo over March 25 to May 18 in Rocky Mountains, Colorado that showing greater change of VIS albedo than that of NIR albedo (Skiles and Painter, 2016). For soil moisture, there was significant negative correlation between soil moisture and SW albedo in August and September. We argue that this pattern can be explained by decreasing contribution of snow cover to SW albedo resulting increasing contribution of soil moisture to SW albedo (Fig. 7). Meanwhile, the increasing contribution of soil moisture to NIR albedo along the aridity gradients from humid to arid region supports that soil moisture plays a more important role in the arid region than that in the humid region.

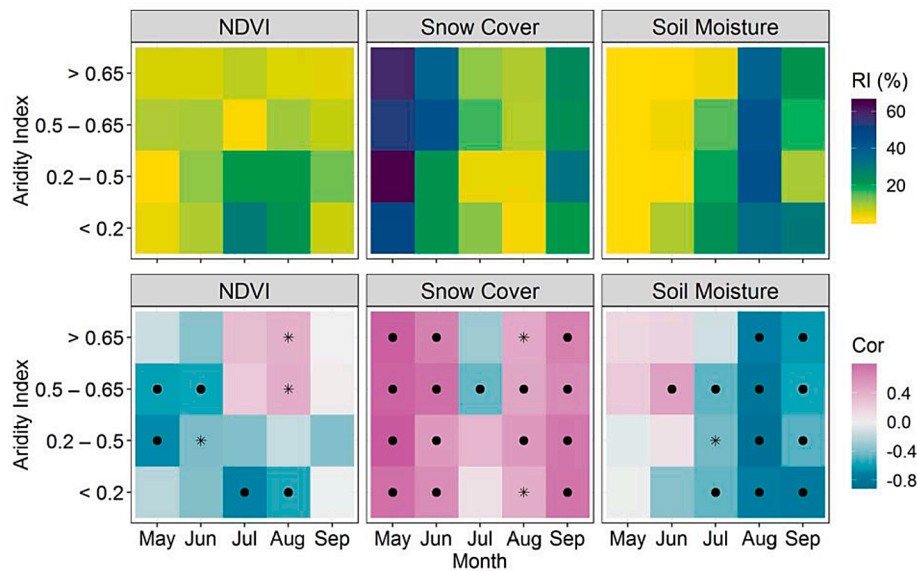


Fig. 7. Relative controls over SW albedo with respect to aridity. Top row shows relative importance (RI) of NDVI, snow cover, and soil moisture to the growing season monthly SW albedo. Bottom row indicates correlation coefficients between the growing season monthly SW albedo and NDVI, snow cover, and soil moisture. The asterisks (*) indicate statistical significance at $p < 0.1$ level, and the black dots indicate significance at $p < 0.05$ level.

4.2. Uncertainties and future needs

Snow albedo is driven mainly by snowfall, surface roughness, metamorphism, and light-absorbing impurities in snow and ice, such as dust and black carbon (Seidel et al., 2016; Skiles and Painter, 2016). The topographic slope has a large influence on the albedo in TP (Lin et al., 2020). In this study, we mainly focused on the albedo change caused by changes in NDVI, snow cover, and soil moisture, while other factors were excluded. As for precipitation, we only considered the amount of precipitation, however, the number of days with snowfall can be equally important for snow albedo by affecting albedo through the amount of fresh snow (Fassnacht et al., 2016). The deep soil moisture cannot be observed by remote sensing could trigger the green-up of vegetation and decrease canopy albedo (Sanchez-Mejia and Papuga, 2014; Sanchez-Mejia et al., 2014), which was not considered in our study.

The phenology of vegetation could have been affected by climate change, since warming has lengthened the growing season in most of TP region (Sun et al., 2015; Zhang et al., 2013a). May and July were important months for vegetation greening, because the rate of increase in NDVI was higher than in other months in the TP (Fig. S5a1, a2). Our results showed that the BGS positively correlated with SW albedo in eastern TP, but most of correlations were insignificant (Fig. 4c), which could indicate that vegetation was not the foremost important factor affecting albedo. The value of surface downward shortwave was highest in May in the TP (Yang et al., 2010a). So, the change of SW albedo in rapid spring transition (May) could have an important impact on surface energy budgets. In addition, the drivers of albedo may vary by time and space, and therefore higher temporal and spatial resolution should be further explored to identify heterogeneous driving factors (Tian et al., 2017). The snow albedo feedback mechanism has important influences on climate on all spatial and temporal scales (Seidel et al., 2016). The combined impacts of vegetation phenology, the number of days with snowfall, snow duration, and air temperature on albedo and surface energy budgets need to be assessed in the future.

5. Conclusion

In this study, we detected spatial, temporal, and spectral variability in albedo due to changes of NDVI, snow cover and soil moisture in the grasslands of TP. We found that 3/4 of grasslands experienced a

greening trend (1/4 significant), while over half of grasslands showed decreasing trends in SW albedo, snow cover, and soil moisture. VIS albedo was more sensitive to change in vegetation greenness than NIR albedo. In most of the grasslands, the VIS albedo was negatively correlated with NDVI throughout the growing season. However, the negative correlation between SW/NIR albedo and NDVI only occurred in limited area. Snow cover was identified as the foremost important driver in May and June, and soil moisture in August. In May and June, the strong correlation between albedo and snow cover in the TP region indicated that decrease in snow cover could contribute more to warming by influencing land surface energy budget in the early growing season. Through analyzing the spatial patterns (aridity gradients) of correlations between NDVI and albedo, we found VIS and NIR albedo counterbalance can further limit the contributions of vegetation greenness to SW albedo in sub-humid and humid region. However, the mechanisms linking the regional climate change are very complex, and therefore more factors of non-radiative mechanisms need to be investigated (e.g., evapotranspiration) and analyzed to support climate change research. The findings in this study can improve our understanding of land-atmosphere interactions in the TP region and are helpful for improving energy budget simulations in land surface models.

Declaration of competing interest

The authors declare that they have no known competing financial interests or personal relationships that could have appeared to influence the work reported in this paper.

Acknowledgments

Major funding for this research was provided under Strategic Priority Research Program of Chinese Academy of Sciences (XDA2006040101), Guangdong Provincial Department of Science and Technology (2019ZT08G090), National Key Research project: "The Tibetan Plateau Land-Air Coupling System Change and Its Global Climate Effect" (No. 91637211), National Key Research and Development Project (2018YFC1507505 and 2016YFC0400902), and Hundred Talent Program.

Supplementary materials

Supplementary material associated with this article can be found, in the online version, at doi:10.1016/j.agrformet.2021.108479.

References

- Abera, T.A., Heiskanen, J., Pellikka, P., Rautiainen, M., Maeda, E.E., 2019. Clarifying the role of radiative mechanisms in the spatio-temporal changes of land surface temperature across the Horn of Africa. *Remote Sens. Environ.* 221, 210–224.
- Abera, T.A., Heiskanen, J., Pellikka, P.K.E., Maeda, E.E., 2020. Impact of rainfall extremes on energy exchange and surface temperature anomalies across biomes in the Horn of Africa. *Agric. For. Meteorol.* 280.
- Alibakhshi, S., Hovi, A., Rautiainen, M., 2019. Temporal dynamics of albedo and climate in the sparse forests of Zagros. *Sci. Total Environ.* 663, 596–609.
- Bai, W., Chen, X., Tang, Y., He, Y., Zheng, Y., 2019. Temporal and spatial changes of soil moisture and its response to temperature and precipitation over the Tibetan Plateau. *Hydrol. Sci. J.* 64 (11), 1370–1384.
- Bonan, G.B., 2008. Forests and climate change: forcings, feedbacks, and the climate benefits of forests. *Science* 320 (5882), 1444–1449.
- Bright, R.M., et al., 2017. Local temperature response to land cover and management change driven by non-radiative processes. *Nat. Clim. Change* 7 (4), 296–302.
- Carrer, D., et al., 2014. Dynamic mapping of snow-free vegetation and bare soil albedos at global 1km scale from 10-year analysis of MODIS satellite products. *Remote Sens. Environ.* 140, 420–432.
- Chen, B., et al., 2014. The impact of climate change and anthropogenic activities on alpine grassland over the Qinghai-Tibet Plateau. *Agric. For. Meteorol.* 189–190, 11–18.
- Chen, D., Loboda, T.V., He, T., Zhang, Y., Liang, S., 2018. Strong cooling induced by stand-replacing fires through albedo in Siberian larch forests. *Sci. Rep.* 8 (1), 4821.
- Chen, X., Long, D., Hong, Y., Liang, S., Hou, A., 2017. Observed radiative cooling over the Tibetan Plateau for the past three decades driven by snow cover-induced surface albedo anomaly. *J. Geophys. Res. Atmos.* 122 (12), 6170–6185.
- Coll, J., Li, X., 2018. Comprehensive accuracy assessment of MODIS daily snow cover products and gap filling methods. *ISPRS J. Photogramm. Remote Sens.* 144, 435–452.
- Didan, K., Barreto, A., 2016. NASA MEaSUREs Vegetation Index and Phenology (VIP) Phenology EVI2 Yearly Global 0.05Deg CMG, distributed by NASA EOSDIS Land Processes DAAC. https://doi.org/10.5067/MEaSUREs/VIP/VIPPHEN_EVI2.004.
- Dorigo, W., et al., 2017. ESA CCI Soil Moisture for improved Earth system understanding: State-of-the-art and future directions. *Remote Sens. Environ.* 203, 185–215.
- Duan, A., Xiao, Z., 2015. Does the climate warming hiatus exist over the Tibetan Plateau? *Scientific Reports* 5 (1).
- Fassnacht, S.R., Cherry, M.L., Venable, N.B.H., Saavedra, F., 2016. Snow and albedo climate change impacts across the United States Northern Great Plains. *The Cryosphere* 10 (1), 329–339.
- Friedl, M.A., et al., 2010. MODIS Collection 5 global land cover: Algorithm refinements and characterization of new datasets. *Remote Sens. Environ.* 114 (1), 168–182.
- Ganjurjav, H., et al., 2016. Differential response of alpine steppe and alpine meadow to climate warming in the central Qinghai-Tibetan Plateau. *Agric. For. Meteorol.* 223, 233–240.
- Gao, Y., Li, X., Leung, L.R., Chen, D., Xu, J., 2015. Aridity changes in the Tibetan Plateau in a warming climate. *Environ. Res. Lett.* 10 (3), 034013.
- Gates, D.M., 1965. Energy, plants, and ecology. *Ecology* 46 (1-2), 1–13.
- Grömping, U., 2006. Relative importance for linear regression in R: the package relaimpo. *J. Stat. Softw.* 17 (1), 1–27.
- Hammerle, A., Haslwanter, A., Tappeiner, U., Cernusca, A., Wohlfahrt, G., 2007. Leaf area controls on energy partitioning of a temperate mountain grassland. *Biogeosciences* 5 (2), 421–431.
- Hou, X., Feng, L., Chen, X., Zhang, Y., 2018. Dynamics of the wetland vegetation in large lakes of the Yangtze Plain in response to both fertilizer consumption and climatic changes. *ISPRS J. Photogramm. Remote Sens.* 141, 148–160.
- Huang, K., et al., 2018. Enhanced peak growth of global vegetation and its key mechanisms. *Nat. Ecol. Evol.* 2 (12), 1897–1905.
- Kala, J., Evans, J.P., Pitman, A.J., Schaaf, C.B., Decker, M., Carouge, C., Mocko, D., Sun, Q., 2014. Implementation of a soil albedo scheme in the CABLEv1.4b land surface model and evaluation against MODIS estimates over Australia. *Geosci. Model Dev.* 7 (5), 2121–2140.
- Kuusinen, N., Stenberg, P., Korhonen, L., Rautiainen, M., Tomppo, E., 2016. Structural factors driving boreal forest albedo in Finland. *Remote Sens. Environ.* 175, 43–51.
- Li, C., et al., 2018a. Spatiotemporal variation of snow cover over the Tibetan Plateau based on MODIS snow product, 2001–2014. *Int. J. Climatol.* 38 (2), 708–728.
- Li, L., et al., 2018b. Current challenges in distinguishing climatic and anthropogenic contributions to alpine grassland variation on the Tibetan Plateau. *Ecol. Evol.* 8 (11), 5949–5963.
- Li, L., et al., 2019. Increasing sensitivity of alpine grasslands to climate variability along an elevational gradient on the Qinghai-Tibet Plateau. *Sci. Total Environ.* 678, 21–29.
- Li, Q., Ma, M., Wu, X., Yang, H., 2018c. Snow Cover and Vegetation-Induced Decrease in Global Albedo From 2002 to 2016. *J. Geophys. Res. Atmos.* 123 (1), 124–138.
- Li, Z., et al., 2018d. The relationship between surface spectral albedo and soil moisture in an arid Gobi area. *Theor. Appl. Climatol.* 136 (3–4), 1475–1482.
- Lin, X., et al., 2020. Spatiotemporal Variability of Land Surface Albedo over the Tibet Plateau from 2001 to 2019. *Remote Sens.* 12 (7).
- Liu, F., Chen, Y., Lu, H., Shao, H., 2017. Albedo indicating land degradation around the Badain Jaran Desert for better land resources utilization. *Sci. Total Environ.* 578, 67–73.
- Loranty, M.M., Goetz, S.J., Beck, P.S.A., 2011. Tundra vegetation effects on pan-Arctic albedo. *Environ. Res. Lett.* 6 (2), 024014.
- Lukeš, P., Stenberg, P., Möttus, M., Manninen, T., Rautiainen, M., 2016. Multidecadal analysis of forest growth and albedo in boreal Finland. *Int. J. Appl. Earth Obs. Geoinf.* 52, 296–305.
- Malmros, J.K., Mernild, S.H., Wilson, R., Tagesson, T., Fensholt, R., 2018. Snow cover and snow albedo changes in the central Andes of Chile and Argentina from daily MODIS observations (2000–2016). *Remote Sens. Environ.* 209, 240–252.
- Meng, X., et al., 2017. Detecting hydrological consistency between soil moisture and precipitation and changes of soil moisture in summer over the Tibetan Plateau. *Clim. Dyn.* 51 (11–12), 4157–4168.
- Moody, E.G., King, M.D., Schaaf, C.B., Hall, D.K., Platnick, S., 2007. Northern Hemisphere five-year average (2000–2004) spectral albedos of surfaces in the presence of snow: Statistics computed from Terra MODIS land products. *Remote Sens. Environ.* 111 (2), 337–345.
- Piao, S., et al., 2012. Impacts of climate and CO2 changes on the vegetation growth and carbon balance of Qinghai-Tibetan grasslands over the past five decades. *Glob. Planet. Change* 98–99, 73–80.
- Planque, C., Carrer, D., Roujean, J.-L., 2017. Analysis of MODIS albedo changes over steady woody covers in France during the period of 2001–2013. *Remote Sens. Environ.* 191, 13–29.
- Pu, Z., Xu, L., Salomonson, V.V., 2007. MODIS/Terra observed seasonal variations of snow cover over the Tibetan Plateau. *Geophys. Res. Lett.* 34 (6).
- Sanchez-Mejia, Z.M., Papuga, S.A., 2014. Observations of a two-layer soil moisture influence on surface energy dynamics and planetary boundary layer characteristics in a semiarid shrubland. *Water Resour. Res.* 50 (1), 306–317.
- Sanchez-Mejia, Z.M., et al., 2014. Quantifying the influence of deep soil moisture on ecosystem albedo: The role of vegetation. *Water Resour. Res.* 50 (5), 4038–4053.
- Seidel, F.C., Ritter, K., Skiles, S.M., Molotch, N.P., Painter, T.H., 2016. Case study of spatial and temporal variability of snow cover, grain size, albedo and radiative forcing in the Sierra Nevada and Rocky Mountain snowpack derived from imaging spectroscopy. *The Cryosphere* 10 (3), 1229–1244.
- Shen, M., et al., 2015. Evaporative Cooling over the Tibetan Plateau Induced by Vegetation Growth, 112. *PNAS*, pp. 9299–9304.
- Skiles, S.M., Painter, T., 2016. Daily evolution in dust and black carbon content, snow grain size, and snow albedo during snowmelt, Rocky Mountains, Colorado. *J. Glaciol.* 63 (237), 118–132.
- Song, J., 1999. Phenological influences on the albedo of prairie grassland and crop fields. *Int. J. Biometeorol.* 42 (3), 153–157.
- Stewart, I.T., 2009. Changes in snowpack and snowmelt runoff for key mountain regions. *Hydrol. Processes* 23 (1), 78–94.
- Sun, W., et al., 2015. Spatiotemporal vegetation cover variations associated with climate change and ecological restoration in the Loess Plateau. *Agric. For. Meteorol.* 209–210, 87–99.
- Tan, K., et al., 2010. Application of the ORCHIDEE global vegetation model to evaluate biomass and soil carbon stocks of Qinghai-Tibetan grasslands. *Global Biogeochemical Cycles* 24 (1) n/a-n/a.
- Tian, L., Zhang, Y., Zhu, J., 2014. Decreased surface albedo driven by denser vegetation on the Tibetan Plateau. *Environ. Res. Lett.* 9 (10), 104001.
- Tian, L., Chen, J., Zhang, Y., 2017. Growing season carries stronger contributions to albedo dynamics on the Tibetan plateau. *PLoS One* 12 (9), e0180559.
- Wang, L., et al., 2018a. Response of surface temperature to afforestation in the Kubuqi Desert, Inner Mongolia. *J. Geophys. Res. Atmos.* 123 (2), 948–964.
- Wang, X., Pang, G., Yang, M., 2018b. Precipitation over the Tibetan Plateau during recent decades: a review based on observations and simulations. *Int. J. Climatol.* 38 (3), 1116–1131.
- Wang, S., Zhang, B., Yang, Q., Chen, G., Yang, B., Lu, L., Shen, M., Peng, Y., 2017a. Responses of net primary productivity to phenological dynamics in the Tibetan Plateau. *China. Agric. For. Meteorol.* 232, 235–246.
- Wang, X., Wu, C., Wang, H., Gonsamo, A., Liu, Z., 2017b. No evidence of widespread decline of snow cover on the Tibetan Plateau over 2000–2015. *Sci. Rep.* 7 (1), 14645.
- Wang, Z., Schaaf, C.B., Sun, Q., Shuai, Y., Román, M.O., 2018c. Capturing rapid land surface dynamics with Collection V006 MODIS BRDF/NBAR/Albedo (MCD43) products. *Remote Sens. Environ.* 207, 50–64.
- Williamson, S.N., Barrio, I.C., Hik, D.S., Gamon, J.A., 2016. Phenology and species determine growing-season albedo increase at the altitudinal limit of shrub growth in the sub-Arctic. *Glob. Chang. Biol.* 22 (11), 3621–3631.
- Wu, J., et al., 2013. Grazing-exclusion effects on aboveground biomass and water-use efficiency of alpine grasslands on the northern Tibetan plateau. *Rangeland Ecol. Manag.* 66 (4), 454–461.
- Xia, J., et al., 2018. Estimates of grassland biomass and turnover time on the Tibetan Plateau. *Environ. Res. Lett.* 13 (1).
- Xiao, L., Che, T., Chen, L., Xie, H., Dai, L., 2017. Quantifying Snow Albedo Radiative Forcing and Its Feedback during 2003–2016. *Remote Sens.* 9 (9).
- Yang, K., He, J., Tang, W., Qin, J., Cheng, C.C.K., 2010a. On downward shortwave and longwave radiations over high altitude regions: Observation and modeling in the Tibetan Plateau. *Agric. For. Meteorol.* 150 (1), 38–46.
- Yang, Y., Fang, J., Fay, P.A., Bell, J.E., Ji, C., 2010b. Rain use efficiency across a precipitation gradient on the Tibetan Plateau. *Geophys. Res. Lett.* 37 (15).
- Yao, T., et al., 2012. Different glacier status with atmospheric circulations in Tibetan Plateau and surroundings. *Nat. Clim. Change* 2 (9), 663–667.

- You, Q., Fraedrich, K., Ren, G., Pepin, N., Kang, S., 2013. Variability of temperature in the Tibetan Plateau based on homogenized surface stations and reanalysis data. *Int. J. Climatol.* 33 (6), 1337–1347.
- Zhang, B., et al., 2012. Effects of rainfall amount and frequency on vegetation growth in a Tibetan alpine meadow. *Climatic Change* 118 (2), 197–212.
- Zhang, G., Zhang, Y., Dong, J., Xiao, X., 2013a. Green-up Dates in the Tibetan Plateau have Continuously Advanced from 1982 to 2011, 110. *PNAS*, pp. 4309–4314.
- Zhang, Y.-f., Wang, X.-p., Hu, R., Pan, Y.-x., Zhang, H., 2013b. Variation of albedo to soil moisture for sand dunes and biological soil crusts in arid desert ecosystems. *Environ. Earth Sci.* 71 (3), 1281–1288.
- Zheng, L., et al., 2019. Spatial, temporal, and spectral variations in albedo due to vegetation changes in China's grasslands. *ISPRS J. Photogramm. Remote Sens.* 152, 1–12.